

Article

# Competitive Evaluation of Planar Embedded Glass and Polymer Waveguides in Data Center Environments

Richard Pitwon <sup>1,\*</sup> , Kai Wang <sup>1</sup>, Akira Yamauchi <sup>2</sup>, Takaaki Ishigure <sup>2</sup>, Henning Schröder <sup>3</sup>, Marcel Neitz <sup>4</sup> and Mayank Singh <sup>5</sup>

<sup>1</sup> Photonics Advanced Research Group, Seagate, Havant, Hampshire PO9 1SA, UK; kai.wang@seagate.com

<sup>2</sup> Department of Applied Physics and Physico-Informatics, Faculty of Science and Technology, Keio University, 3-14-1, Hiyoshi, Kohoku-ku, Yokohama 223-8522, Japan; akiraymch@keio.jp (A.Y.); ishigure@appi.keio.ac.jp (T.I.)

<sup>3</sup> Fraunhofer-Gesellschaft zur Foerderung der Angewandten Forschung e.V, Fraunhofer IZM, Gustav-Meyer-Allee 25, D-13355 Berlin, Germany; henning.schroeder@izm.fraunhofer.de

<sup>4</sup> Technische Universität Berlin, Gustav-Meyer-Allee 25, D-13355 Berlin, Germany; marcel.neitz@izm.fraunhofer.de

<sup>5</sup> Sumitomo Bakelite, Sumitomo Bakelite Co., Ltd., Tennoz Parkside Building 19 F, Shinagawa-ku, Tokyo 140-0002, Japan; mayank@sumibe.co.jp

\* Correspondence: richard.pitwon@seagate.com; Tel.: +44-(0)75-3278-9472

Received: 20 June 2017; Accepted: 1 September 2017; Published: 13 September 2017

**Abstract:** Optical printed circuit board (OPCB) waveguide materials and fabrication methods have advanced considerably over the past 15 years, giving rise to two classes of embedded planar graded index waveguide based on polymer and glass. We consider the performance of these two emerging waveguide classes in view of the anticipated deployment in data center environments of optical transceivers based on directly modulated multimode short wavelength VCSELs against those based on longer wavelength single-mode photonic integrated circuits. We describe the fabrication of graded index polymer waveguides, using the Mosquito and photo-addressing methods, and graded index glass waveguides, using ion diffusion on thin glass foils. A comparative characterization was carried out on the waveguide classes to show a clear reciprocal dependence of the performance of different waveguide classes on wavelength. Furthermore, the different waveguide types were connected into an optically disaggregated data switch and storage system to evaluate and validate their suitability for deployment in future data center environments.

**Keywords:** optical printed circuit board (OPCB); graded index waveguides; polymer waveguides; planar glass waveguides

## 1. Introduction

In order to accommodate spiraling digital data consumption and maximize resource utilization, data centers need to embrace more flexible and scalable topologies, which allow greater disaggregation of compute, storage and memory resources. As a consequence of the resulting need for ubiquitous, distance-agnostic, communication links, future data center systems will increasingly need to accommodate a wider range of different optical communication profiles associated with the different optical interconnect tiers in the data center. At the higher switching tiers of the data center, investment in single-mode fiber infrastructures is increasing, as it is considered future-proof and aligns well with emerging silicon photonic integrated circuit based single-mode optical transceiver and switching technologies. A parallel movement is underway at the sub-rack level with low-cost, commodity transceivers enabling a rack or pod-localized multimode infrastructure to emerge. The proliferation of

low-cost multimode midboard transceivers now offers the renewed prospect of optical links migrating into traditionally cost sensitive data center sub-system enclosures. Although, in the early stages of their deployment, these transceivers would be internally connected by commercial fiber jumpers, they will set the crucial precedent for system-embedded optical interconnect in high volume commercial systems. This, in turn, will be expected to provide a fresh entry point for electro-optical printed circuit board (OPCB) technologies whereby optical signals may be conveyed along waveguides embedded within the PCB itself. However, the optimal choice of waveguide type will vary depending on the characteristics of the optical communication signal in question, in particular the wavelength and data rate.

OPCB technology has advanced considerably over the past 15 years with new optical waveguide materials and fabrication techniques providing enhanced performance including reduced signal dispersion through graded refractive index profiles and lower material absorption in different wavelength bands. In particular, two distinct classes of planar graded index multimode waveguide have recently emerged based on polymer [1,2] and glass [3] materials.

This paper provides a review the state of the art in planar graded index waveguides. We report on the fabrication of planar graded index polymer waveguides using the Mosquito method [1] devised by Keio University and the photo-addressing method devised by Sumitomo Bakelite [2], and the fabrication of planar graded index glass waveguides using ion diffusion on thin glass foils as developed by Fraunhofer IZM [4]. We comparatively characterize their insertion loss at both 850 nm and 1310 nm and signal integrity at 10.3 Gb/s to assess their suitability with respect to two emerging transceiver classes based on directly modulated multimode 850 nm VCSELs and single-mode 1310 nm silicon photonic integrated circuits.

The different classes of waveguide were temporarily inserted into an optically disaggregated data storage system using the Serial Attached SCSI protocol and the system performance was characterized to assess their suitability within real future data center environments.

Early comparative research between polymer and glass planar waveguides was reported in [5], and is taken further in this paper to include all leading varieties of embedded planar graded index waveguide.

## 2. Fabrication of Graded Index Polymer Waveguides

### 2.1. Mosquito Fabrication Method (Keio University)

An innovative method of fabricating polymer waveguides with circular cores was developed by Keio University [1]. According to the “Mosquito method”, core monomer is dispensed directly into a layer of cladding monomer. The core and cladding monomers are then both cured simultaneously, which simplifies the fabrication process. The fabrication process steps are outlined in Figure 1: A cladding monomer liquid with a given refractive index is first coated onto the substrate. A core monomer with a higher refractive index than that of the cladding monomer is placed into a syringe, which is mounted on a robotic arm. The tip of the syringe needle is then inserted into the liquid cladding monomer layer to the desired depth at which the waveguide is to be deposited. The robotic arm then moves the syringe tip in the plane of the substrate, while injecting the core monomer out of it at a constant pressure along the entire path of the planned waveguide. Once expelled and drawn out by the moving needle tip, the liquid core monomer coalesces into a cylindrical form suspended within the bulk liquid cladding monomer. This form is maintained along the entire path of the planned waveguide, but as both core and cladding monomers are in a liquid state, they continue to diffuse slightly into each other, giving rise to a graduated concentration distribution of core monomer from the center of the cylindrical construct into the cladding monomer. This in turn is reflected by a corresponding graduated decrease in refractive index from that of the core monomer in the center of the cylindrical construct to that of the cladding monomer at the edges. The robotic arm then repeats the process for subsequent waveguides. Once all cylindrical structures have been dispensed in their liquid form, then the whole substrate is exposed to UV light and the graduated cylindrical forms of

liquid core monomer are partially cured into place to form the waveguides. The substrate is then baked to complete the curing process.

The refractive index profile is determined by the amount of time core and cladding monomers are allowed to diffuse into each other. Therefore, by careful choice of the time between dispensing the core monomer and the curing step, one can tune the refractive index profile of the resulting waveguides to achieve a parabolic graded index profile. Greater control of the refractive index profiles can be achieved by altering other configurable parameters including choice of core and cladding materials, core monomer dispensing pressure and amending the scanning programme. It has been demonstrated that the graded index circular waveguides produced through this method outperform step index waveguides of similar size [6].

Various types of UV curable resins have been used to produce Mosquito waveguides reported in this paper including silicone resin FX-712 (core) and FX-712 (cladding) from ADEKA Corp. (Tokyo, Japan) [7] and an organic–inorganic hybrid resins from Nissan Chemical Ind., Ltd. (Tokyo, Japan), NP-005 (core) and NP-208 (clad) [8].

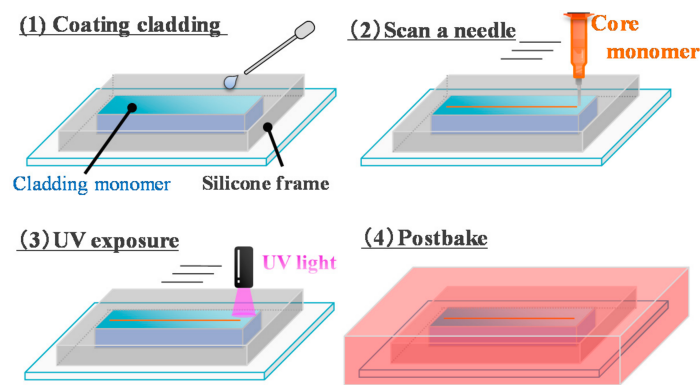


Figure 1. Procedures in the Mosquito method.

Figure 2 shows various cross-sections of the Mosquito waveguides characterized in this paper. The scanning trails of the needle are clearly visible under the circular graded index core.

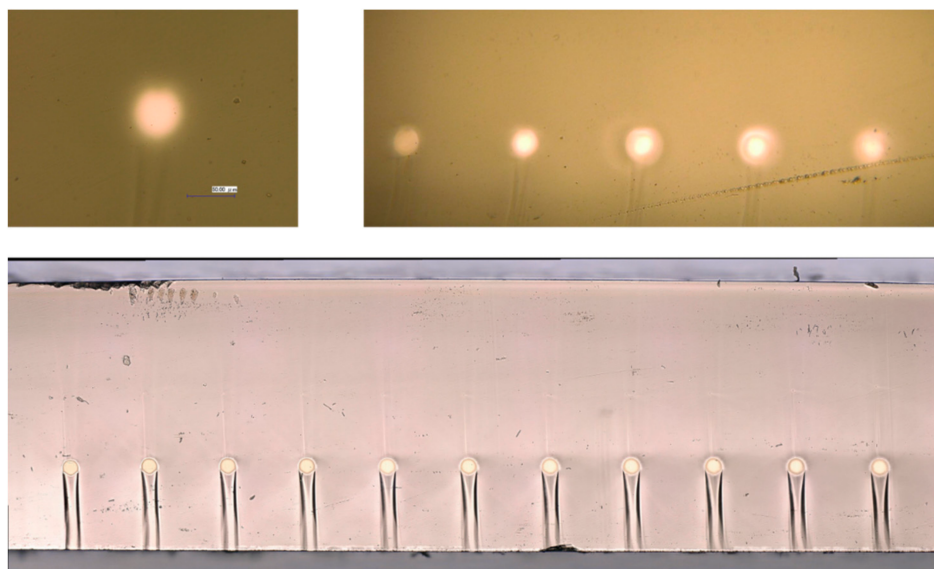
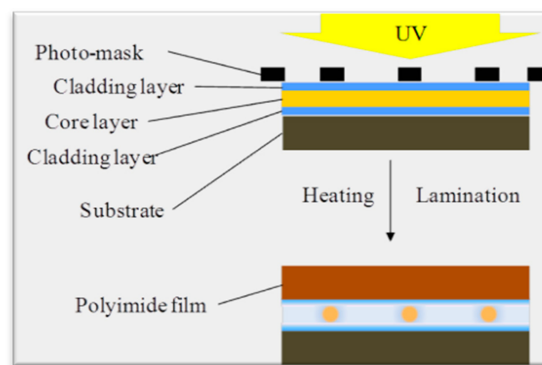


Figure 2. Cross-section of Mosquito GI waveguides.

### 2.2. Photo-Addressing Fabrication Method (Sumitomo Bakelite)

Sumitomo Bakelite developed a fabrication process for graded index polymer waveguides, which is based on the photo-addressing method. The details of the photo addressing method are outlined in Figure 3.



**Figure 3.** Graded index waveguide fabrication.

A special varnish is prepared for the polymer core and cladding layers and coated onto a substrate. Special refractive index modifiers and photo initiators are incorporated into the varnish prior to use. These refractive index modifiers and initiators catalyze the production of graded refractive index profiles in the fabricated waveguides. The coated layers are then pre-baked, exposed to UV light through a photo-mask and heated to a certain temperature to obtain graded index polymer waveguide [9]. After heat treatment, the waveguide is laminated with polyimide film to protect it from the outer environment. Figure 4 shows the cross-sectional image of GI core waveguide after fabrication.

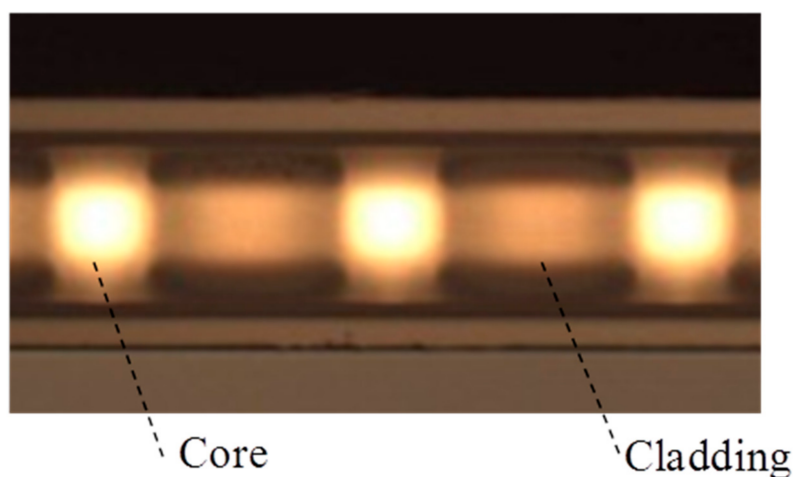


**Figure 4.** Cross section of addressed GI waveguides.

Sumitomo Bakelite have developed a method of terminating polymer waveguides with a parallel optical ferrule, which is compliant with a single row 12 channel MT ferrule. The Polymer MT or PMT ferrule is currently being deployed in various commercial products by Sumitomo Bakelite (Tokyo, Japan) (Figure 5).



**Figure 5.** Photo-addressed waveguide termination of photo-addressed waveguides with PMT connector (left side) and out-of-plane coupling array (right end) Source: Sumitomo Bakelite.

### 2.3. Waveguide Crossovers

One limitation of the Mosquito waveguides compared to the photo-addressed waveguides is that the Mosquito waveguides cannot be crossed through each other directly as is common with most planar embedded polymer waveguides including the photo-addressed waveguides. Figure 6 shows a photo of a photo-addressed waveguide layout with multiple waveguide cross-overs at multiple angles. The Mosquito waveguides can however be made to cross past each other as this method allows waveguide heights to be changed over the course of the waveguide.



**Figure 6.** Photo-addressed waveguides with waveguide layout showing multiple cross-overs at varied crossing angles (Source: Sumitomo Bakelite).

## 3. Fabrication of Graded Index Glass Waveguides (Fraunhofer IZM)

### 3.1. Two-Step Ion Diffusion Fabrication Process

The glass waveguide fabrication consists of a two-step thermal ion-exchange process between salt-melt and display glass suitable for large panel and batch processing. The glass waveguide panel processing line at Fraunhofer IZM (Berlin, Germany) is shown in Figure 7. Process steps like sputtering (PVD), lithography (Dip-Coater, LDI, etc.) and glass panel separation (Laser-Cutter) are suitable for board formats of up to  $610 \times 457 \text{ mm}^2$ . The glass panel areas that can be processed this way are limited to  $305 \times 457 \text{ mm}^2$ . Fraunhofer IZM have already processed waveguide panels with a maximum size of  $305 \times 440 \text{ mm}^2$ .



**Figure 7.** Fraunhofer IZM glass panel waveguide process line.

The test waveguides produced for this research were patterned on chemically untreated Corning Gorilla Glass 1 (distributed by Schröder Spezialglas, Ellerau, Germany), which was only available in a thickness of 550  $\mu\text{m}$ . The glass waveguides were fabricated as follows. An aluminum layer of 400 nm thickness was deposited on both the top and bottom surfaces of the glass foil through DC-sputtering by Creavac Creamet 600 physical vapor deposition (PVD) equipment (Creavac, Dresden, Germany). The glass panel was then dip coated to deposit photoresist on both sides of the panel and the top surface patterned by an Orbotec Paragon Ultra 200 laser direct imaging (LDI) system (Orbotec, Tokyo, Japan), which transferred the waveguide layout and alignment mark patterns to the photoresist layer, the uncured areas subsequently being developed away. Then, the exposed aluminum layer on the top-surface was etched through an acid treatment and the photoresist removed completely. The glass panel was vertically lowered into a furnace containing a hot salt melt. The salt melt for the first diffusion step comprised a diluted  $\text{AgNO}_3$  mixture. During this step, sodium ions in the glass matrix were exchanged with silver ions in the salt mixture, giving rise to a localized graduated increase in the refractive index of the glass. The concentration gradient of the silver ions into the bulk glass was proportional to the resulting refractive index gradient with the highest refractive index change occurring at the exposed glass surface interface to the mixture and the refractive index decreasing in a graduated manner to that of the bulk glass. This gave rise to an isotropic refractive index profile emanating from the exposed glass panel section. The aluminum mask layers were subsequently removed from the top and bottom glass surfaces by wet chemical etching. A single step ion diffusion process of glass waveguide fabrication was reported by Karabchevsky [10] for sensing applications, whereby the refractive index maxima was on the top surface of the glass, however for optical communication applications a second ion diffusion step is required to generate a graded index profile with the index maxima buried in the glass. In order, therefore, to “round off” the waveguide profile and shift the refractive index maximum to a certain depth below the glass surface, a second ion diffusion step was implemented whereby salt ions were leached back out of the glass matrix into a second solution. Following this two-step ion diffusion process, an MDI LD600-H system  $\text{CO}_2$ -laser scribing system (Mainz, Germany) was used to score the glass panel into smaller sections with identical waveguide layouts. The individual sections were then manually snapped off along the score lines, producing very high-quality facets. This process is described in more detail in the next section. The test waveguides had a length of 190 mm and each glass section contained one group of 12 parallel straight waveguides with a center-to-center channel pitch of 250  $\mu\text{m}$ . By varying the process parameters, one can vary the characteristics of the waveguide including the waveguide dimension, NA and distance of the maximum refractive index point from the glass surface, which in turn will affect the coupling and propagation losses of the waveguide.

To this end, two different sets of test waveguide samples were produced with different diffusion times and silver salt melt concentration. These sets were given the internal designations “set 1” and “set 7” as the intervening five sample set processes were not completed. In particular the diffusion time from parameter set 7 was longer than that of set 1. Refractive near field (RNF) scans were conducted on both sets of waveguides to determine their cross-sectional refractive index profiles. Figure 8a,b respectively show the horizontal refractive index profiles of set 1 and set 7. Waveguides fabricated according to parameter set 1 showed a refractive index maximum shifted to a depth of around 15  $\mu\text{m}$  below the glass surface, while for waveguides fabricated according to parameter set 7, the index maximum was shifted to a depth of 30  $\mu\text{m}$ . The refractive index differences measured between core center and cladding were 0.025 for set 1 and 0.029 for set 7 with corresponding NAs of 0.27 and 0.3 respectively, and the size of the set 1 waveguides are smaller than that of the set 7 waveguides. These relative waveguide characteristics are an expected consequence of the longer diffusion time in set 7.

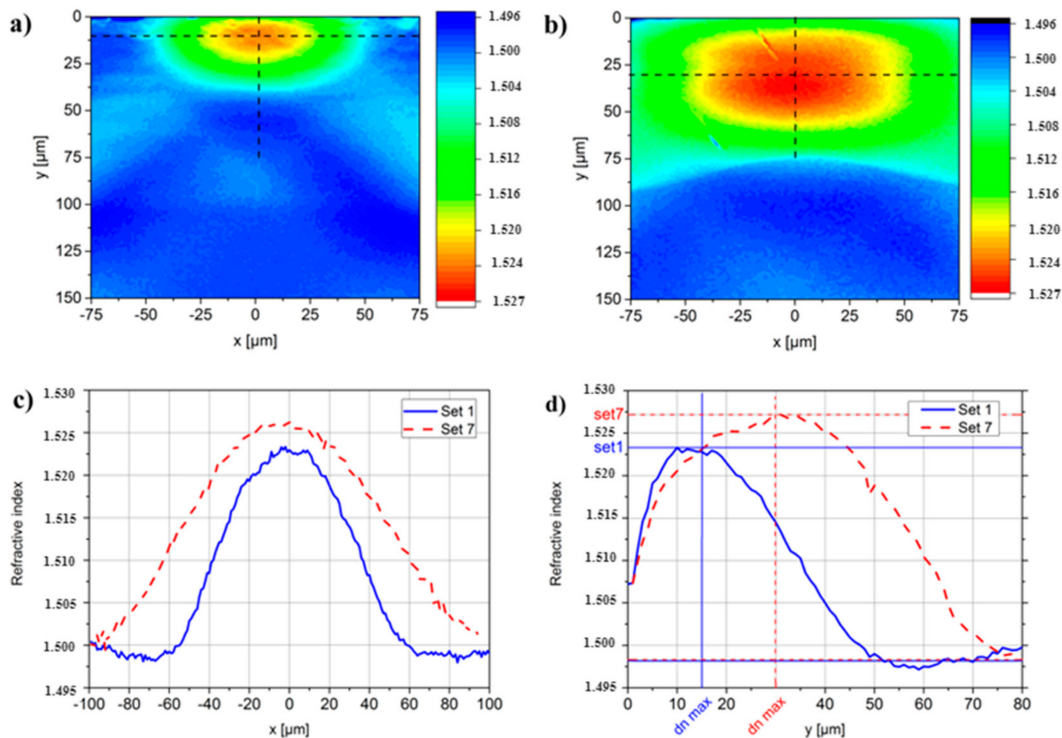


**Figure 8.** Refractive index profiles of selected glass waveguides with fabrication parameter sets 1 and 7: (a) Refractive index near field (RNF) scan of waveguide cross-section from parameter set 1, (b) RNF scan of waveguide from parameter set 7, (c) refractive index profiles along the horizontal axis of sets 1 and 7, (d) refractive index profiles along the vertical axis of sets 1 and 7.

### 3.2. End Facet Quality Analysis on Glass Waveguides

The quality of the processed end facets depends on several aspects including layout and process parameters. As mentioned above, the method used by Fraunhofer IZM to cleanly dissect the glass was laser dicing by CO<sub>2</sub>-laser and a cooling nozzle, whereby the glass panel was scored with the laser and subsequently cooled so it could be cleanly snapped, providing optical quality surface finish without subsequent polishing. This process was developed for display glasses with a homogeneous glass matrix, however since the glass matrix is selectively changed by the ion exchange process, a non-homogeneous material profile is created at the cut-line and this must be considered. In order to mitigate any deleterious effects of direct laser exposure to the waveguides themselves, the laser scoring process takes place on the opposite surface of the glass panel to the surface where the glass waveguides were formed. The laser dicing process was followed by manual glass separation, which comprised snapping the glass at the interface using a scoring and snapping principle. This method, however, is not only dependent on the cut- and waveguide-process, but also on the operator. Therefore, repeatability of the process would be variable.

To investigate this issue, IZM followed the well-known cut-back procedure to comparatively characterize the end-facet coupling loss performance on both glass waveguide sample sets under test. The cut-back measurement results are shown in Figure 9 and the derivation of propagation loss is shown in Table 1. Measurements were made in accordance with IEC measurement standard [11].

These results indicate a strong dependence of the coupling and propagation losses of ion-diffused glass waveguides on the NA and core size.

Unneglectable are also the comparatively large error bars for most of the measurements. Even for set 7 with lower errors, measurements at 1310 nm are only meaningful because of the measurement at the shortest length. Nevertheless, a conclusion can be drawn that the cut-back procedure gave good insight into the value of the measurement data on IZM's straight waveguides. Besides this

investigation, another issue should be investigated in the future: Due to the change of the ion-radius during the thermal diffusion step, small sodium ions ( $\text{Na}^+$ ) are replaced by much larger silver ions ( $\text{Ag}^+$ ). This results in tension due to higher mechanical stresses within the waveguide vicinities. These tensions are not a reliability issue, but pose a risk for varying pitch densities. The crack during manual breaking, after the laser dicing process, propagates from one side of the glass interface to the other as required. This crack, however, will be disturbed by high changes of density. Thus, high amounts of silver, e.g., due to a small pitch, a large array or several small arrays can give rise to a larger variation in end facet quality during the breaking process. This influence was discovered during processing of the glass used in this paper and is currently undergoing further investigation.

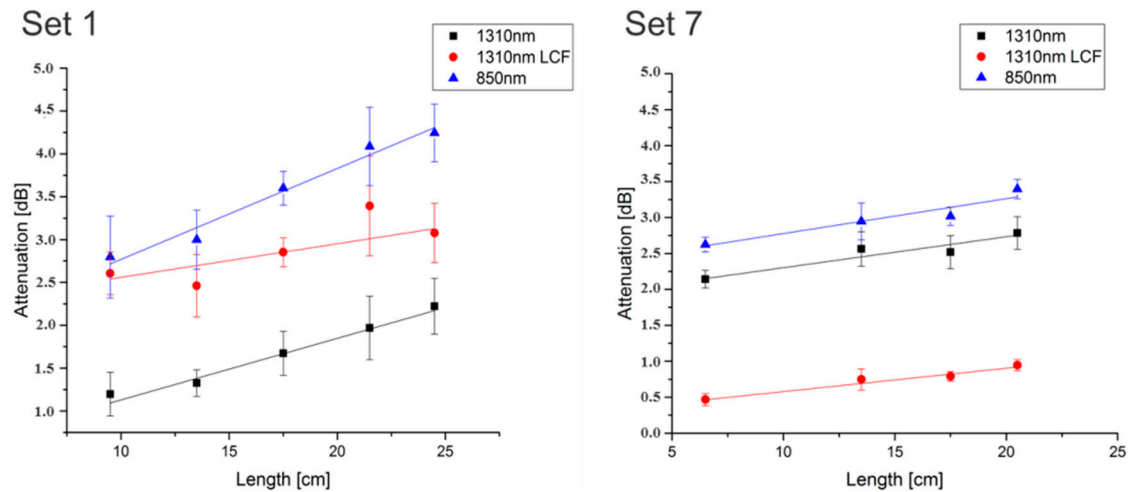


**Figure 9.** Cut-back measurements on both glass waveguide samples under test to compare end facet coupling losses at both 1310 nm and 850 nm with a standard fiber launch and 1310 nm only with a large core fiber (200  $\mu\text{m}$ ) launch in accordance with IEC measurement standard [11].

**Table 1.** Derivation of Insertion Loss (IL) and Propagation Loss (PL) from cut-back measurements.

Wavelength	Set 1		Set 7	
GI 50 launch fiber	PL (dB/cm)	IL (dB)	PL (dB/cm)	IL (dB)
850 nm	$0.11 \pm 0.01$	$1.71 \pm 0.19$	$0.05 \pm 0.01$	$2.29 \pm 0.14$
1310 nm	$0.07 \pm 0.008$	$0.41 \pm 0.12$	$0.04 \pm 0.008$	$0.25 \pm 0.1$
Large Core Fiber	Set 1		Set 7	
850 nm	$0.04 \pm 0.014$	$2.17 \pm 0.24$	$0.03 \pm 0.004$	$1.87 \pm 0.06$

#### 4. Optical Measurement Process

##### 4.1. Optical Waveguide Measurement Set-Up

Insertion loss measurements on the test waveguides were carried out at Seagate by both Seagate and Keio University staff using the measurement set-up shown in Figure 10. This is one of the principal multimode fiber launch configurations recommended in the optical circuit board measurement standard: “IEC 62496-2—General guidance for definition of measurement conditions for optical characteristics of optical circuit boards” [11]. The continuous wave optical output from a commercial 850 nm source was conveyed along 50/125  $\mu\text{m}$  OM3 graded-index multimode fiber (GI-MMF) through an Arden Photonics Modcon mode conditioner to produce an encircled flux (EF) profile at the fiber launch facet, which complies with the EF profile defined in the international standard IEC 61280-4-1 [12]. The output of the waveguide under test was collected by an integrated sphere photodetector through an OM2 GI-MMF fiber. The reference power for the insertion loss measurements was obtained by butt-coupling the input and output fibers together and measured to be  $-8.87$  dBm. Both input and

output fibers were end-fire coupled to the input and output waveguide facets respectively with no refractive index matching oil applied. The input and output fibers were held in a brace on an x–y–z translation stage to provide accurate mechanical alignment.

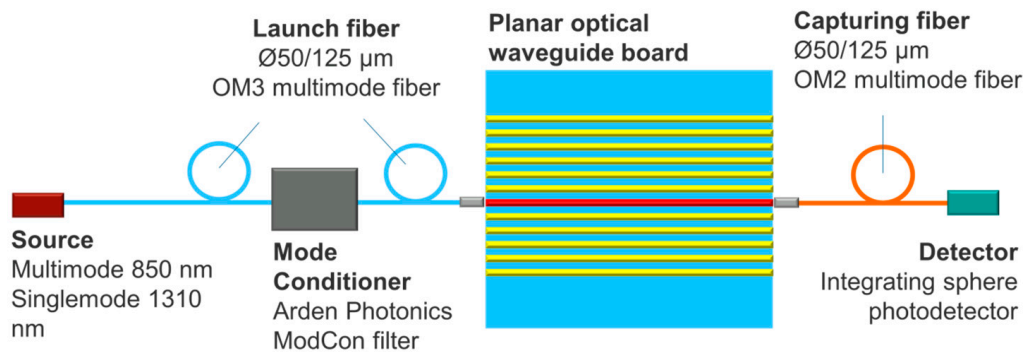


Figure 10. Measurement schematic of the multimode fiber launch.

#### 4.2. Comparative Insertion Loss Measurements at 850 nm and 1310 nm

The parameters for the different waveguides under test are shown in Table 2.

Table 2. Polymer and glass waveguide parameters.

Parameters	Mosquito Waveguides	Sumitomo Waveguides	Glass Waveguides	
Core, $n_1$	(NP-005), 1.597	-	Set 1 1.523	Set 7 1.527
Cladding, $n_2$	(NP-208), 1.569	-	1.498	1.498
Index difference	0.028		0.025	0.029
Sample length	5 cm	17.6 cm	19 cm	19 cm
Optical layer thickness	0.5 mm	0.1 mm	0.55 mm	0.55 mm
Core size	~50 µm	~50 µm	~50 µm	~50 µm
Channel Pitch	250 µm	250 µm	250 µm	250 µm
Fab. method	Mosquito	Photo addressing	Ion diffusion	Ion diffusion
Index Profile	GI	GI	Elliptical GI	Elliptical GI

Table 3 shows the average insertion losses measured on the planar graded index polymer Mosquito and photo-addressed waveguides, and the planar graded index glass waveguides at wavelengths of 850 nm and 1310 nm. Unfortunately, due to damage of the photo-addressed sample, measurements of the photo-addressed waveguides at 1310 nm could not be completed, so are excluded from the results presented.

Table 3. Average insertion loss measured at 850 nm and 1310 nm on glass and polymer waveguides under test.

Input Wavelength (nm)	Insertion Loss (dB)			
	Mosquito Waveguide	Photo-addressed Waveguide	Glass Waveguide	
			Set 1	Set 7
850	2.73 ± 0.69	3.32 ± 0.31	4.90 ± 0.32	4.23 ± 0.20
1310	4.32 ± 0.67	Not available	2.81 ± 0.13	3.00 ± 0.21

The insertion loss per cm is shown in Figure 11 and the insertion loss results are shown in Figure 12.



requirements [11]: OM3 GI-MMF is used for both launch and capturing fibers (50GI–50GI) and a standard single-mode fiber is used for the launch fiber (SMF–50GI). Meanwhile, Figure 14 shows the interim time dependence of the output Near Field Pattern (NFP) from the waveguide. From Figure 14, the insertion loss monotonically decreases with respect to the interim time from 0 to 270 s under both conditions. Then, once the minimum insertion loss is observed at 300- to 430-s interim time, a gradual increase is observed with increasing the interim time. From Figure 14, it is found that the core-cladding boundary in the cross-section becomes blurred with increasing interim time, which means the refractive index gradation is gradually formed. By comparing the NFP image to the scale bar of 50  $\mu\text{m}$  in Figure 14, it is also found that originally the output optical field of the NFP is slightly larger than the designed core diameter (50  $\mu\text{m}$ ). Since the core has a profile close to an SI when the interim time is short, the NFP is widely spread to the whole core in the first two cores, even if the core is launched with a small beam spot via an SMF. Therefore, the insertion losses are as high as 1.8 to 3 dB when the interim time is shorter than 105 s, due to the core size and optical field mismatching between the cores of waveguide and GI-MMF (50GI, capturing fiber). Meanwhile, after an interim time of longer than 205 s, the size of output NFPs are almost the same and smaller than 50  $\mu\text{m}$  under 50GI and SMF launch conditions, respectively, although the actual core diameter observed from the cross section is much larger than 50  $\mu\text{m}$  due to the monomer diffusion. The small spot of the output NFP is a well-known feature of the GI core, which leads to a high efficiency coupling to the GI-MMF capturing fiber. Hence, the low insertion loss is observed after an interim time longer than 205 s, as shown in Figure 14. Here, the insertion loss slightly increases when the interim time is long enough (longer than 500 s). The excess diffusion of the core and cladding monomers contributes to the decrease of the NA of the core, resulting in lowering the light confinement effect. From the NFPs of the last two cores in Figure 14, a gradual spot size increment is visually observed.

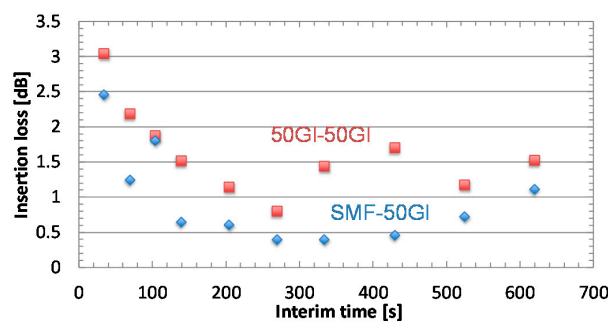


Figure 13. Interim time dependence of the insertion loss of the 5-cm long polymer waveguide.

Interim time	34.5 s	105 s	205 s	335 s	430 s	620 s
Cross Section						
NFP: SMF launch	 50 $\mu\text{m}$					
Loss (dB)	2.457	1.8	0.604	0.398	0.456	1.112
NFP: 50GI launch	 50 $\mu\text{m}$					
Loss (dB)	3.042	1.877	1.14	1.438	1.701	1.521

Figure 14. Interim time dependence of the cross-section, Near Field Pattern (NFP) and insertion loss of the polymer waveguide.

From the above investigation, it is revealed that the insertion loss of the GI core polymer waveguides fabricated using the Mosquito method is sensitive to the index profile, namely the diffusion time for core and cladding monomers. The loss result in Figure 12 shows the similar tendency: Ch. 1 and 2, and Ch. 11 and 12 show higher insertion loss, corresponding to long and short interim times, respectively. (The high loss in Ch. 6 could be accidental.) Therefore, in order to maintain the low insertion loss for all the parallel cores, control of the monomer diffusion is a key issue. The group of Keio University is currently investigating how to manage the diffusion from both material and process points of view.

The insertion loss variations measured on the photo-addressed waveguides however are, on average, lower than those of Mosquito waveguides with the exception that photo-addressed waveguide 4 was damaged so no result was recorded. On the glass waveguides under test, the waveguides fabricated according to parameter set 1 exhibited lower loss at 1310 nm than those fabricated by parameter set 7. However, the set 7 waveguides exhibited lower loss at 850 nm than the set 1 waveguides. This implies that the glass waveguide fabrication parameters can be tuned to a given operational wavelength.

The planar polymer Mosquito waveguides under test consistently showed lower insertion loss at 850 nm than at 1310 nm, while the planar glass waveguides under test consistently showed a lower insertion loss at 1310 nm than at 850 nm.

In glass waveguides, the insertion losses at 850 nm are higher than at 1310 nm, due to the formation of silver ion clusters in the glass matrix, which induce stronger intrinsic scattering at 850 nm than at 1310 nm. This effect can be mitigated by changing the glass composition and improving the waveguide process.

In polymer waveguides, the insertion losses at 1310 nm are higher than at 850 nm due to the intrinsic absorption profile of the polymer material, which is particularly affected by the vibration frequency of the C–H bonds in the polymer material [13].

#### 4.4. Signal Integrity Characterization

The signal integrity characterization set-up shown in Figure 15 is described as follows. A 10.3125 Gb/s PRBS  $2^{31}-1$  test pattern was generated by an Anritsu MT1810 pulse pattern generator (PPG) and used to drive either a commercial 850 nm or 1310 nm XFP transceiver. As with the insertion loss measurements, a mode conditioner was used to ensure the near field modal distribution at the fiber launch complied with the EF requirements set out in IEC 61280-4-1<sup>13</sup>. The output from the waveguide was conveyed by an OM2 fiber through a variable optical attenuator into a Tektronix CSA8000B communications signal analyzer (CSA). By selection of either the 850 nm or 1310 nm XFP transceiver, signal integrity measurements were carried out at 850 nm for polymer and 1310 nm for glass waveguides. Back-to-back signal integrity reference measurements were carried out for each wavelength, whereby a variable optical attenuator (VOA) was used to adjust the signal power amplitude received at the CSA to be equal to the measured power for each given waveguide measurement in order to compensate for any jitter dependence of the CSA on received power levels.

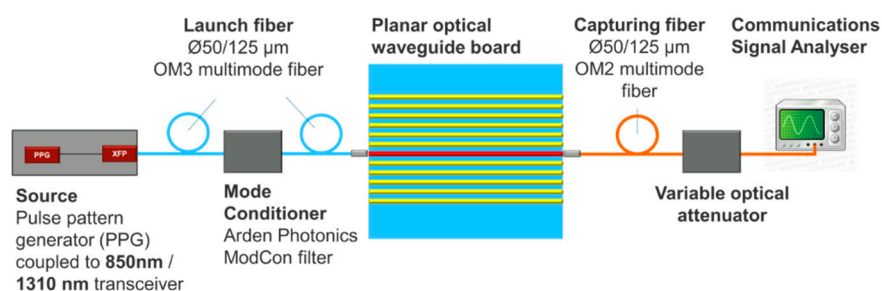
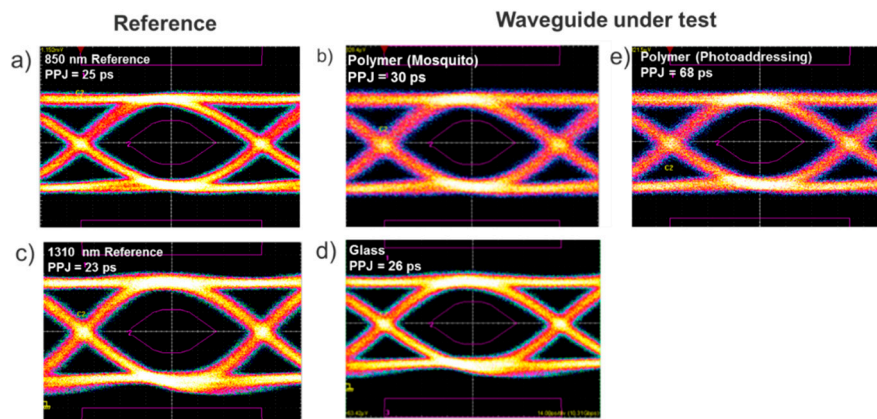


Figure 15. Signal integrity measurement set-up.

Figure 16 shows eye diagrams of the waveguides under test at their respective best operating wavelength (1310 nm for glass waveguides, 850 nm for both types of polymer waveguides) with minimal added signal distortion apparent.



**Figure 16.** Eye diagrams for 10.3 Gb/s with the PRBS  $2^{31}-1$  test signal conveyed over selected polymer and glass waveguides, (a) 850 nm reference eye diagram with direct fiber coupled to a communications signal analyzer (CSA), (b) Mosquito waveguide channel 5 at 850 nm, (c) 1310 nm reference eye diagram with direct fiber coupled to a CSA, (d) IZM glass waveguide set 7 channel 12 at 1310 nm; (e) Photo-addressed waveguide channel 7 at 850 nm.

Bit Error Rate testing was also carried out on the waveguides at their respective best operational wavelengths using an Anritsu MT1810 signal analyzer (Anritsu Corporation, Tokyo, Japan). A bit error rate of less than  $10^{-12}$  was measured on all waveguides.

## 5. Validation of Different Waveguide Classes in an Optically Enabled Data Center System

Figure 17 shows an optically enabled data storage array system, which was designed and developed on the PhoxTroT project. The PhoxTest03.01 platform (Seagate, Havant, UK) was based on an existing 2U (89 mm) high, 19" wide Seagate OneStor™ system enclosure.

PhoxTest03.01 includes two optically enabled 12 G SAS switch controller modules, an electro-optical midplane based on a 192 fiber flexplane and 24 optically enabled 2.5" Small Form Factor hard disk drives. All devices and links in the system are 12 G capable and have been fully characterized and validated using appropriate SAS device detection and soak test regimes as reported in a previous paper [14].

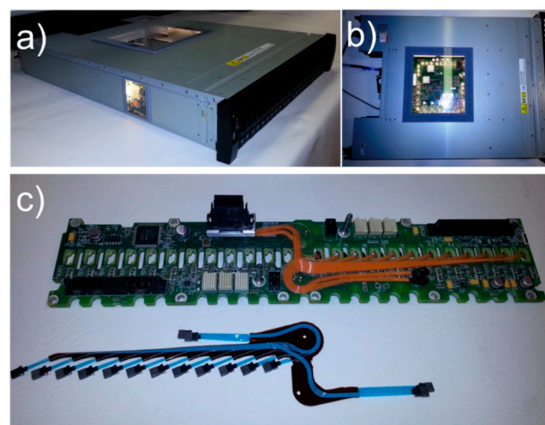


**Figure 17.** PhoxTest03.01 data storage platform: (a) Fully populated enclosure in operation, (b) top view of the enclosure, (c) electro-optical midplane with fiber flexplane.

### 5.1. System Level Measurement Set-Up

The PhoxTest03.01 platform allows the suitability of different waveguide types to be assessed, when incorporated in an optically disaggregated data center environment. The measurement set-up is shown in Figure 18. The optical fiber under test connected from the board mounted optical transceiver is passed to the same mechanical brace and alignment stage used in the measurement set-ups described in Figures 10 and 15 to align accurately to one end of the waveguide under test. The optical fiber from the standard midplane connector is passed to the other end of the waveguide under test and mounted in a mechanical brace and alignment stage, allowing it to be aligned accurately to the waveguide facet.

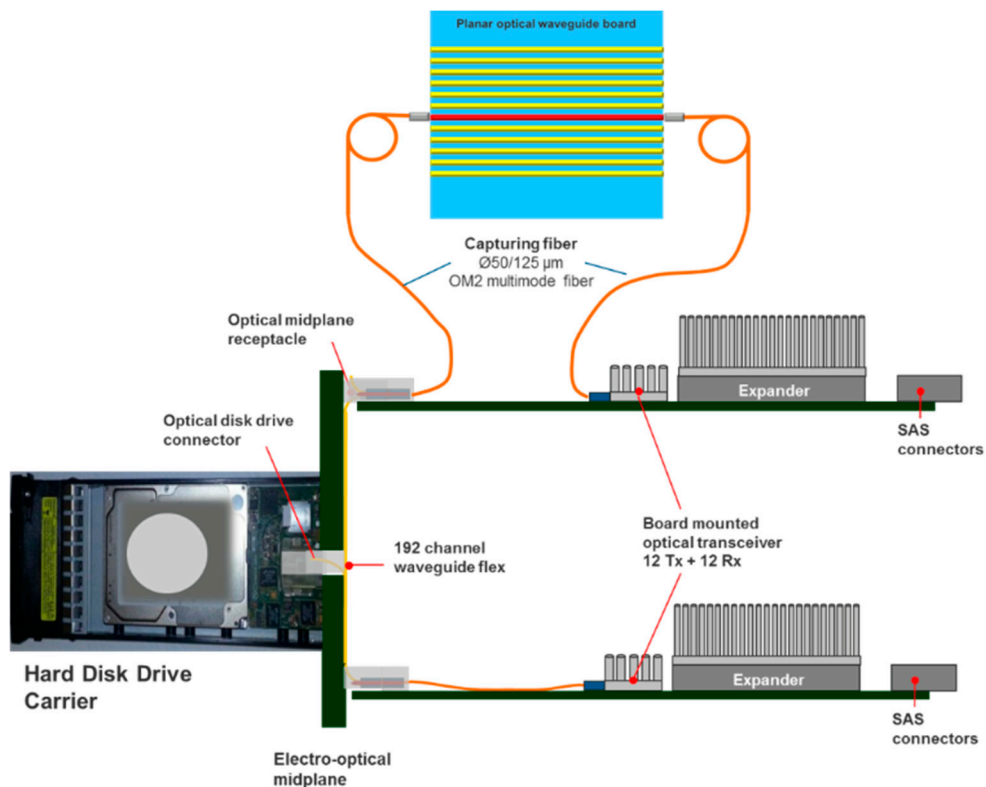


**Figure 18.** System level measurement set-up showing the optically enabled system schematic with waveguides under test connected to the intra-system optical network.

### 5.2. System Level Measurement Results

Each waveguide under test was connected between the 850 nm optical interface of a Finisar BOA midboard optical transceiver (Finisar, Wuxi, China) connected directly to a Serial Attached SCSI (SAS) expander switch (Microsemi, Aliso Viejo, CA, USA) via the electro-optical midplane connection to one optically enabled 6 Gb/s SAS disk drive. The performance of the system with the connected drive was characterised using IOmeter (Open Source Development Labs, San Francisco, CA, USA), an open source I/O subsystem measurement and characterization tool for single and clustered systems [15]. The waveguide channels with the lowest insertion loss were chosen for the Mosquito (channel 5) and glass waveguide (set 7, channel 12). On the photo-addressed waveguide test board, a waveguide with a median insertion loss (channel 1) was chosen. The IOmeter system performance graphs in Figure 19 show the number of error-free data transfers in MB/s per data block size. Negligible difference in system performance is observed by inserting the waveguide section into the system. Although, this is expected given the short waveguide lengths and relatively low losses, it demonstrates that system level performance as a whole is not adversely affected, providing system level validation, in addition to channel level validation of at least short lengths of optical waveguide.

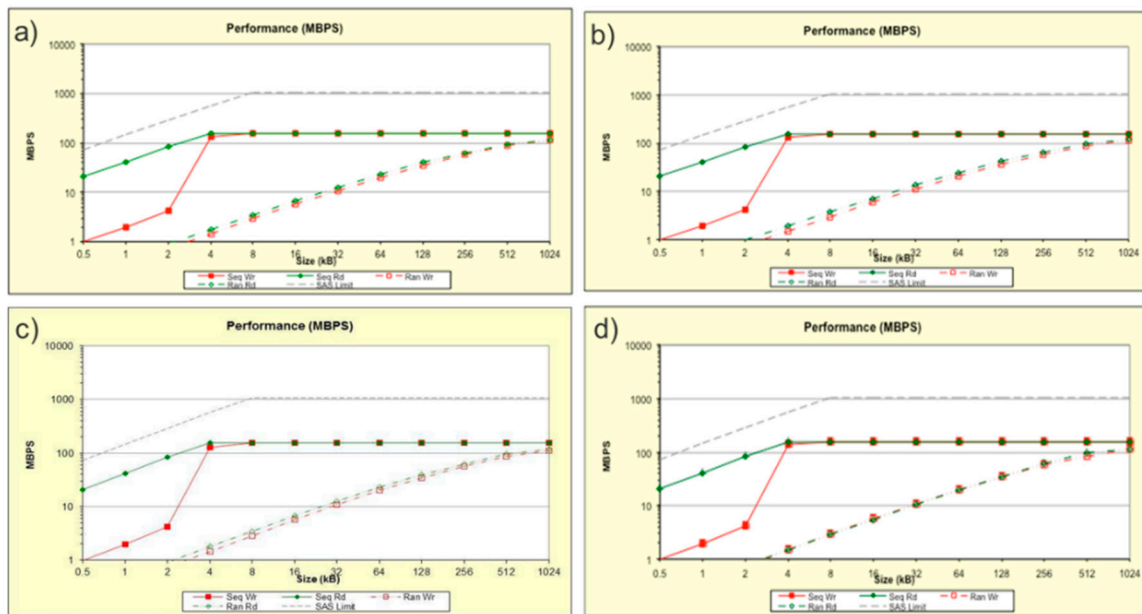


**Figure 19.** Optically enabled data storage system performance in terms of error-free data transfers per data block size with different waveguides connected to the system. (a) reference measurement with fiber only system, (b) Keio mosquito waveguide channel 5 operating at 850 nm, (c) Sumitomo Bakelite waveguide channel 1 operating at 850 nm, (d) IZM glass waveguide set 7 channel 12 at 850 nm.

## 6. Conclusions

In this paper, we have reported on the comparative characterization between two leading classes of multimode planar optical waveguide, namely graded index polymer waveguides produced using the Mosquito and Photo-addressing methods, and planar graded index glass waveguides produced using an ion diffusion method. The insertion loss measurements at the key communications wavelengths of 850 nm and 1310 nm showed a consistent reciprocal relationship between the two waveguide material types with respect to wavelength, with polymer waveguides showing lower insertion loss at 850 nm than at 1310 nm, and glass waveguides showing lower insertion loss at 1310 nm than at 850 nm. Signal integrity and bit error rate measurements on both waveguide classes indicated low added signal distortion at their respective optimal wavelengths and a bit error rate of less than  $10^{-12}$ . The waveguides were incorporated into an optically enabled data center platform and system level characterization was carried out showing negligible performance disruption from any of the waveguides at 850 nm. The fact that the state-of-the-art in embedded graded index waveguides of both classes has been validated in the prototype platform paves the way for widespread deployment of both emerging classes of embedded graded index waveguide in future optically enabled data center systems.

**Acknowledgments:** The research reported herein was carried out as part of the EU H2020 project “COSMICC” (grant agreement No. 688516) and EU FP7 project “PhoxTrot” (grant agreement No. 318240), for which it has received funding from the European Union.

**Author Contributions:** Richard Pitwon, Henning Schröder, Takaaki Ishigure and Mayank Singh conceived and designed the experiments. Akira Yamauchi, Kai Wang and Marcel Neitz performed the experiments and analysed the data. Richard Pitwon, Takaaki Ishigure, Mayank Singh, Henning Schröder and Marcel Neitz wrote the paper.

**Conflicts of Interest:** The authors declare no conflict of interest.

## References

1. Soma, K.; Ishigure, T. Fabrication of a Graded-Index Circular-Core Polymer Parallel Optical Waveguide Using a Microdispenser for a High-Density Optical Printed Circuit Board. *IEEE J. Sel. Top. Quantum Electron.* **2013**, *19*, 3600310. [CrossRef]
2. Ito, Y.; Terada, S.; Singh, M.K.; Arai, S.; Choki, K. Demonstration of High-Bandwidth Data Transmission above 240 Gbps for Optoelectronic Module with Low-Loss and Low-Crosstalk Polynorborene Waveguides. In Proceedings of the 2012 IEEE 62nd Electronic Components and Technology Conference (ECTC), San Diego, CA, USA, 29 May–1 June 2012; pp. 1526–1531.
3. Brusberg, L.; Schröder, H.; Herbst, C.; Frey, C.; Fiebig, C.; Zakharian, A.; Kuchinsky, S.; Liu, X.; Fortusini, D.; Evans, A. High Performance Ion-Exchanged Integrated Waveguides in Thin Glass for Board-Level Multimode Optical Interconnects. In Proceedings of the 2015 European Conference on Optical Communication (ECOC), Valencia, Spain, 27 September–1 October 2015.
4. Pitwon, R.; Brusberg, L.; Schroeder, H.; Whalley, S.; Wang, K.; Miller, A.; Cole, A. Pluggable Electro-Optical Circuit Board Interconnect Based on Embedded Graded-Index Planar Glass Waveguides. *J. Light Technol.* **2015**, *33*, 741–754. [CrossRef]
5. Pitwon, R.; Yamauchi, A.; Brusberg, L.; Wang, K.; Ishigure, T.; Schröder, H.; Neitz, M.; Worrall, A. Planar Polymer and Glass Graded Index Waveguides for Data Center Applications. *Opt. Interconnects XIV* **2016**, 9753. [CrossRef]
6. Ishigure, T. Graded-index core polymer optical waveguide for high-bandwidth-density optical printed circuit boards: Fabrication and characterization. *Opt. Interconnects XIV* **2014**, 8991, 899102–899110. [CrossRef]
7. Adeka Corporation. Available online: <https://www.adk.co.jp/en> (accessed on 1 August 2017).
8. Ishigure, T.; Yoshida, S.; Yasuhara, K.; Suganuma, D. Low-loss single-mode polymer optical waveguide at 1550-nm wavelength compatible with silicon photonics. In Proceedings of the 2015 IEEE 65th Electron Components Technology Conference, San Diego, CA, USA, 26–29 May 2015; pp. 768–774.
9. Horimoto, A.; Kitazoe, K.; Kinoshita, R. Simple channel reconnection using polynorborene based GI waveguide for optical interconnect. In Proceedings of the 2015 IEEE CPMT Symposium Japan (ICSJ), Kyoto, Japan, 9–11 November 2015; pp. 122–125.
10. Karabchevsky, A.; Kavokin, A.V. Giant absorption of light by molecular vibrations on a chip. *Sci. Rep.* **2016**, *6*, 21201. [CrossRef] [PubMed]
11. International Electro-Technical Commission. IEC 62496-2:2017 Optical Circuit Boards—Basic Test and Measurement Procedures—Part 2: General Guidance for Definition of Measurement Conditions for Optical Characteristics of Optical Circuit Boards. 2017. Available online: <https://webstore.iec.ch/publication/32157> (accessed on 1 June 2017).
12. International Electro-technical Commission. IEC 61280-4-1:2009 Fibre-Optic Communication Subsystem Test Procedures—Part 4-1: Installed Cable Plant—Multimode Attenuation Measurement; International Electro-Technical Commission: Geneva, Switzerland, 2009.
13. Watanabe, T.; Ooba, N.; Hayashida, S.; Kurihara, T.; Imamura, S. Polymeric Optical Waveguide Circuits Formed Using Silicone Resin. *J. Light Technol.* **1998**, *16*, 1049. [CrossRef]
14. Pitwon, R.; Worrall, A.; Stevens, P.; Miller, A.; Wang, K.; Schmidtke, K. Demonstration of fully enabled data center subsystem with embedded optical interconnect. *Opt. Interconnects XIV* **2014**, 8991, 899110. [CrossRef]
15. Intel Corporation. Iometer Project. Available online: <http://www.iometer.org/> (accessed on 11 January 2016).



© 2017 by the authors. Licensee MDPI, Basel, Switzerland. This article is an open access article distributed under the terms and conditions of the Creative Commons Attribution (CC BY) license (<http://creativecommons.org/licenses/by/4.0/>).